RSC Advances

ROYAL SOCIETY OF CHEMISTRY

www.rsc.org/advances

Cite this: DOI: 10.1039/c0xx00000x

www.rsc.org/xxxxxx

ARTICLE TYPE

Band gap engineering design for construction of energy-levels well-matched semiconductor heterojunction with enhanced visible-light-driven photocatalytic activity

Hongwei Huang[a,]*, Shuobo Wang [a], Yihe Zhang[a,]*, Paul K. Chu[b]

Received (in XXX, XXX) Xth XXXXXXXXX 20XX, Accepted Xth XXXXXXXXX 20XX

DOI: 10.1039/b000000x

Energy-levels well-matched $Mg_{1-x}Cu_xWO_4$ (0.1<x<0.5)/Bi_2WO_6 heterojunctions with Type II staggered conduction bands and valence bands have been successfully constructed through band gap engineering based on solid-solution design and synthesized by a facile one-step hydrothermal method. X-ray diffraction (XRD), X-ray photoelectron spectroscopy (XPS), scanning electron microscopy (SEM), transmission electron microscopy (TEM), high-resolution transmission electron microscopy (HRTEM) and UV−vis diffuse reflectance spectra (DRS) were utilized to characterize the crystal structures, morphologies and optical properties of the as-prepared products. The as-designed $Mg_{0.7}Cu_{0.3}WO_4/Bi_2WO_6$ heterojunctions consisting of nanocubes and nanoplates structures exhibit much higher visible-light-driven (VLD) photocatalytic activity than the two individuals for the degradation of RhB and photocurrent generation. The photoluminescence (PL) spectra, photoelectrochemical measurement, active species trapping and quantification experiments all indicated that the fabrication of energy-levels well-matched overlapping band-structures can greatly facilitate the separation and easy transfer of photo-generated electrons and holes, thus resulting in the remarkably enhanced photocatalytic activity. This work provides a novel strategy for semiconductor heterojunction construction and energy-band structure regulation.

Introduction

Semiconductor photocatalysis technique is receiving great attention due to their potential applications in organic contamination treatment for environmental remediation.[1-3] However, the application of traditional photocatalysts, e.g. TiO_2, ZnO was limited by their incapable visible-light absorption, though they may exhibit excellent photocatalytic performance under UV irradiation.[4-6] To cope with these problems, great efforts have been made on the development of new photocatalysts with visible light response and improvement of the photocatalytic activity.[7,8] Among these strategies, fabrication of heterojunction photocatalysts by coupling of two semiconductors with appropriate energy band levels has been a significant approach, that can effectively separate and transfer the photogenerated electron−hole pairs, thus resulting in high photocatalytic activity.[9-11] Nevertheless, construction of a heterojunction system demands that the energy band levels of the two semiconductors must be overlapping well-matched. Therefore, the most crucial problem of constructing a heterojunction is to seek coupling photocatalysts with matched conduction band (CB) and valence band (VB).

Recently, bismuth tungstate (Bi_2WO_6) as a most studied example of the Aurivillius oxide family with perovskite-like structure exhibits excellent photocatalytic performance under visible light, which can be ascribed to its layered structure and moderate band gap (2.6～2.8 eV).[12,13] In order to further improve the photocatalytic activity of Bi_2WO_6, various modification were adopted, including element doping (such as F, B, Fe, Mo, etc.)[14-17] and especially coupling with heterogeneous semiconductors, for instance, TiO_2/Bi_2WO_6,[18] $ZnWO_4/Bi_2WO_6$,[19] WO_3/Bi_2WO_6,[20] $BiOI/Bi_2WO_6$,[21] C_3N_4/Bi_2WO_6[22] and $BiIO_4/Bi_2WO_6$.[23] Here, we describe a novel design strategy to develop visible-light-driven (VLD) heterojunction system with Bi_2WO_6 by utilizing the tungstate solid-solution $Mg_{1-x}Cu_xWO_4$ for the following considerations: (1) The narrow band-gap semiconductor $CuWO_4$ ensures the absorption of visible light.[24] (2) Compared with the big electronegativity of Zn atom (4.45 eV) and Cd atom (4.33 eV), the much smaller electronegativity of Mg atom (3.75 eV) than Cu atom (4.48 eV) could adjust the CB and VB position and might construct overlapping band-structures of heterojunction. (3) As belonging to tungstate family, they can be developed via facile one-step hydrothermal method.

In this study, the above considerations have been successfully fulfilled. We have prepared $Mg_{0.7}Cu_{0.3}WO_4/Bi_2WO_6$ composite photocatalysts consisting of $Mg_{0.7}Cu_{0.3}WO_4$ nanocubes decorated with Bi_2WO_6 nanoplates by one-step hydrothermal method. Under visible light irradiation, the $Mg_{0.7}Cu_{0.3}WO_4/Bi_2WO_6$

composite exhibited much higher photocatalytic activity than those of two individuals, which was verified by the photodegradation of rhodamine B (RhB) and photoelectrochemical measurements. The enhancement of VLD photocatalytic activity was ascribed to the high separation efficiency of photogenerated electron−hole pairs at the intimate interface of heterojunctions.Experimental Section

2. Experimental Section

2.1 Materials and Synthesis Procedure.

The raw materials $Bi(NO_3)_3·5H_2O$, $Mg(NO_3)_2·6H_2O$, $Cu(NO_3)_2·6H_2O$ and $Na_2WO_4·2H_2O$ as well as other reagents including tetraacetic acid disodium salt (EDTA-2Na), iso-propanol (IPA), benzoquinone (BQ) and nitroblue tetrazolium (NBT) from commercial sources were all AR grade and used as received without further purification. $Mg_{1-x}Cu_xWO_4$ (x=0, 0.1, 0.2 0.3 0.4 and 1) and $Mg_{0.7}Cu_{0.3}WO_4/Bi_2WO_6$ samples were synthesized by a hydrothermal method.

In a typical synthesis of $Mg_{1-x}Cu_xWO_4$ (x=0, 0.1, 0.2 0.3 0.4 and 1), total amounts of 0.001mol of $Mg(NO_3)_2·6H_2O$ and $Cu(NO_3)_2·6H_2O$ (molar numbers of 0.001:0, 0.0009:0.0001, 0.0008:0.0002, 0.0007:0.0003, 0.0006:0.0004 and 0:0.001, respectively) were dissolved in 30 ml deionized water, and the breaker was placed in an ultrasonic bath for 10 min to dissolve raw materials. Meanwhile, 0.001mol $Na_2WO_4·2H_2O$ were dissolved in 30 ml deionized water to obtain a clear solution. Then, the solution was mixed and then stirred for 3 h at room temperature. The resulting suspension was subsequently transferred into a 100 ml Teflon-lined stainless autoclave and heated at 180 ℃ for 24 h. After cooling, the products were collected by filtration and washed repeatedly with deionized water, and then dried at 60 ℃ for 12 h.

In a typical synthesis of $Mg_{0.7}Cu_{0.3}WO_4/Bi_2WO_6$ sample with molar ratio 1:4, 0.008 $Bi(NO_3)_3·5H_2O$, 0.0007mol $Mg(NO_3)_2·6H_2O$ and 0.0003mol $Cu(NO_3)_2·6H_2O$ were added to 30 ml deionized water, and the breaker was placed in an ultrasonic bath for 10 min to dissolve raw materials. Meanwhile, 0.005mol $Na_2WO_4·2H_2O$ were dissolved in 30 ml deionized water to obtain a clear solution. Then, the solution was mixed, and then stirred for 3 h. The resulting suspension was subsequently transferred into a 100 ml Teflon-lined stainless autoclave and heated at 180 ℃ for 24 h. After cooling, the products were collected by filtration and washed repeatedly with deionized wate, and then dried at 60 ℃ for 12 h. According to this method, different molar ratios of $Mg_{0.7}Cu_{0.3}WO_4/Bi_2WO_6$ samples at 1:2, 1:6 and 1:10 were prepared, respectively. The pure Bi_2WO_6 samples were also synthesized under the same conditions as references.

2.2 Catalyst characterization

Powder X-ray diffraction (XRD) was performed on an X/max-rA Advance diffractometer with Cu Kα radiation. X-ray photoelectron spectroscopy (XPS) with Al Ka X-rays (ht = 1486.6 eV) irradiation operating at 150 W was employed to investigate the chemical composition and surface properties of the samples. A S-4800 scanning electron microscopy (SEM) was used to observe the general morphology and microstructure of the products. Transmission electron microscopy (TEM) and high-resolution transmission electron microscopy (HRTEM) analyses were performed using a JEM-2100F electron microscopy (JEOL, Japan). A PerkinElmer Lambda 35 UV–vis spectrometer was utilized to record the UV-vis diffuse reflectance spectra (DRS). The photoluminescence (PL) spectra were measured on a JOBIN 10 YVON FluoroMax-3 fluorescence spectrophotometer with a 150 W Xenon lamp as the excitation lamp.

2.3 Photocatalytic Activity Experiment

Photocatalytic activities of $Mg_{0.7}Cu_{0.3}WO_4$, Bi_2WO_6 and $Mg_{0.7}Cu_{0.3}WO_4/Bi_2WO_6$ heterojunctions were evaluated by decomposition of RhB under visible light irradiation with a 1000 W xenon lamp ($\lambda > 420$ nm). A total of 50 mg of as-prepared photocatalyst was dispersed in an aqueous solution of RhB (50 mL, 0.01 mM). First, the dye solution and photocatalyst were strongly magnetically stirred in the dark for 1 h to get the adsorption-desorption equilibrium. Under irradiation, about 2 mL of the suspension was taken at given time intervals, and then was separated by centrifugation. The concentration of RhB was analyzed by recording the absorbance at the characteristic band of 553 nm using a Cary 5000 UV−vis spectrophotometer.

2.4 Photoelectrochemical Measurements

Photoelectrochemical measurements were carried out in a three-electrode system with a 0.1 M Na_2SO_4 electrolyte solution. Saturated calomel electrodes (SCE) and platinum wire were used as the reference electrodes and counter electrode, respectively. The working electrodes are Bi_2WO_6 and 1:4 $Mg_{0.7}Cu_{0.3}WO_4/Bi_2WO_6$ film electrodes. The photoelectrochemical measurements were performed on an electrochemical system (CHI-660B, China) with light intensity 1 mW/cm^2. The photocurrent (PC) generation and electrochemical impedance spectra (EIS) of the photocatalysts as visible light on and off were measured at 0.0 V. A 5 mV sinusoidal ac perturbation was applied to the electrode over the frequency range of 0.05−105 Hz.

2.5 Active Species Trapping and $•O^{2-}$ Quantification Experiments

To detect the active species generated in the photocatalytic reaction, various scavengers, including 1 mM BQ (a quencher of $•O_2^-$), 1.0 mM IPA (a quencher of •OH) and 1 mM EDTA-2Na (a quencher of h^+) were added.[25,26] The method was similar to the former photocatalytic activity experiment. NBT (0.025 mM, exhibiting an absorption maximum at 259 nm) was utilized to determine the amount of $•O_2^-$ generated from $Mg_{0.7}Cu_{0.3}WO_4/Bi_2WO_6$ heterogeneous. The production of $•O_2^-$ was quantitatively analyzed through recording the concentration of NBT with an UV−vis spectrophotometer. This method was also similar to the former photocatalytic activity and active species trapping experiments with NBT replacing the RhB.

3. Results and discussion

3.1 Band gap engineering design of $Mg_{1-x}Cu_xWO_4$ solid-solution and $Mg_{0.7}Cu_{0.3}WO_4/Bi_2WO_6$ heterojunctions

The ultraviolet-visible diffuse reflectance spectra of $Mg_{1-x}Cu_xWO_4$ (x=0, 0.1, 0.2 0.3 0.4 and 1) samples are displayed in

Fig. 1a. In semiconductors, the square of absorption coefficient is linear with energy for direct optical transitions in the absorption edge region; whereas the square root of absorption coefficient is linear with energy for indirect transitions.[27] The absorption edges of $MgWO_4$ and $CuWO_4$ are caused by direct and indirect transitions, respectively.[28] Since the visible light absorption of Bi_2WO_6 was caused by band gap transition,[29] the band gap of Bi_2WO_6 was estimated from the plot of absorption *vs* energy (Fig. S1). As the energy levels of $MgWO_4$ and $CuWO_4$ are not matched with that of Bi_2WO_6 (Fig. 1c), they could not form effective heterojunctions favoring the separation and transfer of charge carrier. In order to construct energy level matched band-structures, the solid solution of $Mg_{1-x}Cu_xWO_4$ was synthesized to adjust the energy band structure, especially the position of conduction band (CB) and valence band (VB). When the amount of Mg is larger than Cu ($x \leq 0.4$) in the solid solution of $Mg_{1-x}Cu_xWO_4$, it possesses direct band gap.

The band positions of semiconductors can be predicted using electronegativity concept, and the CB and VB potentials of the semiconductor at the point of zero charge can be calculated by the following equation[30]:

$$E_{VB}=X-E^{e}+0.5E_{g} \qquad (1)$$

$$E_{CB}=E_{VB}-E_{g} \qquad (2)$$

where X is the absolute electronegativity of the semiconductors, which is defined as the geometric average of the absolute electronegativity of the constituent atoms, E^e is the energy of free electrons on the hydrogen scale (≈4.5 eV), and E_g is the band gap.[2,30] Band gaps of $Mg_{1-x}Cu_xWO_4$(x=0, 0.1, 0.2 0.3 and 0.4) are determined from the data plots of absorption^2 versus energy in the absorption edge region (Fig. 1b), and the CB and VB were also estimated (Table S1). Fig. 1c presented the energy band of $Mg_{1-x}Cu_xWO_4$ and Bi_2WO_6, it can be seen that the band matched overlapping band-structures between $Mg_{1-x}Cu_xWO_4$ and Bi_2WO_6 have been fabricated when x is between 0.1 and 0.4.

Fig. 2 displayed the UV–vis DRS spectra of $Mg_{0.7}Cu_{0.3}WO_4$, Bi_2WO_6, and $Mg_{0.7}Cu_{0.3}WO_4/Bi_2WO_6$ heterostructures. The absorption edge of pure Bi_2WO_6 is located at about 450 nm in the visible region while that of $Mg_{0.7}Cu_{0.3}WO_4$ is approximate to 550 nm. In contrast, all of the $Mg_{0.7}Cu_{0.3}WO_4/Bi_2WO_6$ heterostructures all exhibit red-shifts on the absorption edges compared with pure Bi_2WO_6, and their edges range from 450 to 550 nm.

3.2 Characterization on $Mg_{0.7}Cu_{0.3}WO_4/Bi_2WO_6$ heterojunctions

As presented in Fig. 3a, orthorhombic phase Bi_2WO_6 with space group Pca2 possesses an Aurivillius layered structure, which is composed of $[Bi_2O_2]^{2+}$ layers together with WO_6 octahedron between them. Shown in Fig. 3b is the schematic crystal structure of monoclinic phase $Mg_{1-x}Cu_xWO_4$. It is composed of $Mg_{1-x}Cu_xO_6$ and WO_6 octahedron. Judged from the crystal structure, $Mg_{1-x}Cu_xWO_4$ may display cube-like surface morphology. X-ray powder diffraction (XRD) was utilized to verify the $Mg_{1-x}Cu_xWO_4$ (x=0, 0.1, 0.2 0.3 0.4 and 1) solid-solution as shown in Fig. 4a. It is obvious that $MgWO_4$, $Mg_{0.9}Cu_{0.1}WO_4$, $Mg_{0.8}Cu_{0.2}WO_4$, $Mg_{0.7}Cu_{0.3}WO_4$, $Mg_{0.6}Cu_{0.4}WO_4$ and $CuWO_4$ with monoclinic structure were successfully synthesized. Moreover, it can also be seen that the diffraction peaks of $Mg_{1-x}Cu_xWO_4$ solid-solution shift from the 2θ position of $MgWO_4$ to that of $CuWO_4$ with the increase of Cu content, further indicating the successful preparation of $Mg_{1-x}Cu_xWO_4$ (x=0, 0.1, 0.2 0.3 0.4 and 1) series.

Fig. 4b depicts the XRD patterns of the as-prepared $Mg_{0.7}Cu_{0.3}WO_4$, Bi_2WO_6 and $Mg_{0.7}Cu_{0.3}WO_4/Bi_2WO_6$ heterojunctions. From the image, it can be seen that the pure Bi_2WO_6 sample exhibits high purity and crystallinity. The diffraction peaks can be identified as the orthorhombic phase of Bi_2WO_6 (PDF#39-0256). Due to the high content and intensity of Bi_2WO_6 diffraction peaks, the $Mg_{0.7}Cu_{0.3}WO_4/Bi_2WO_6$ heterojunctions with molar ratio < 1:4 display similar diffractions to the pure Bi_2WO_6.[22] In the $Mg_{0.7}Cu_{0.3}WO_4/Bi_2WO_6$ composites with molar ratios 1:4 and 1:2, the characteristic diffraction peaks of $Mg_{0.7}Cu_{0.3}WO_4$ were successfully detected, confirming the co-existence of both $Mg_{0.7}Cu_{0.3}WO_4$ and Bi_2WO_6.

The X-ray photoelectron spectroscopy (XPS) analysis was employed to investigate the chemical composition and surface chemical states of the $Mg_{0.7}Cu_{0.3}WO_4/Bi_2WO_6$ heterostructures. The typical survey XPS spectrum indicates that Bi, W, O, Mg and Cu elements could be detected for the 1:4 $Mg_{0.7}Cu_{0.3}WO_4/Bi_2WO_6$ heterostructure (Fig. 5a). The XPS peak for C 1s (285 eV) is ascribed to the adventitious hydrocarbon from the XPS instrument. Fig. 5b-5f show the high resolution XPS spectra. As shown in Fig. 5b, the binding energies of W $4f_{7/2}$ and W $4f_{5/2}$ located at 37.6 and 35.5 eV, respectively.[31] Two strong peaks at 159.4 and 164.7 eV with difference (delta) in binding energies of 5.35 eV shown in Fig. 5c are attributed to Bi $4f_{7/2}$ and Bi $4f_{5/2}$, respectively, which are characteristic of Bi^{3+} in Bi_2WO_6.[32] The O 1s peaks for the $Mg_{0.7}Cu_{0.3}WO_4/Bi_2WO_6$ heterostructure (Fig. 5d) can be deconvoluted into three peaks at 530.1 eV, 531.2 eV and 532.5 eV, which correspond to the lattice oxygen, -OH hydroxyl groups and chemisorbed water, respectively.[16] As for the high-resolution Mg and Cu XPS spectra (Fig. 5e and 5f, respectively), two peaks at 1303.0 eV and 935.1 eV are associated with Mg 1s[33] and Cu 2p3/2,[34] respectively. The XPS results further confirmed the coexistence of $Mg_{0.7}Cu_{0.3}WO_4$ and Bi_2WO_6 in the $Mg_{0.7}Cu_{0.3}WO_4/Bi_2WO_6$ heterostructures.

To further confirm the composition of the heterojunctions quantitatively, ICP elemental analyses are performed on $Mg_{0.7}Cu_{0.3}WO_4/Bi_2WO_6$ products. The results (Table S2) showed that the molar ratios of Mg: Cu: Bi: W are in accorddance with the expected values.

The surface morphology of $Mg_{0.7}Cu_{0.3}WO_4/Bi_2WO_6$ with molar ratios 1:0, 1:2, 1:4, 1:6, 1:10 and 0:1 has been observed by scanning electron microscopy (SEM) as shown in Fig. 6. It can be seen that $Mg_{0.7}Cu_{0.3}WO_4$ (Fig. 6a) and Bi_2WO_6 (Fig. 6f) possess nanocubes and nanoplates structures, respectively. With the increase of the $Bi_2WO_6/Mg_{0.7}Cu_{0.3}WO_4$ molar ratio, the content of the nanoplates also increased (Fig. 6a-6d). Fig. 6c and S2 showed that the as-prepared products of $Mg_{0.7}Cu_{0.3}WO_4/Bi_2WO_6$ with molar ratio 1:4 consist of irregular nanocubes and nanoplates, and the crystal dimension of the nanocubes was estimated to be from several tens of nanometers to one micron, and the thicknesses of these nanosheets of Bi_2WO_6 are in the range of 40-50 nm (Fig. S2). The $Mg_{0.7}Cu_{0.3}WO_4/Bi_2WO_6$ heterojunction was further characterized by TEM. The low magnification TEM images in Fig. 7a and 7b confirmed the nanocubes and nanoplates morphologies of the sample. The high-resolution transmission electron microscopy (HRTEM) image (Fig. 7c) and fast Fourier transform (FFT) images (Fig. 7d and Fig. 7f) confirmed the single crystal nature of $Mg_{0.7}Cu_{0.3}WO_4$ and Bi_2WO_6. The lattice resolved HRTEM image indicates that the spacing of the lattice is 0.181 and 0.310 nm (as seen in Fig. 7e and 7g, respectively), which is consistent with the spacing of the corresponding (022) and (131) planes of orthorhombic monoclinic $Mg_{0.7}Cu_{0.3}WO_4$ and Bi_2WO_6, respectively. The interface between Bi_2WO_6 and $Mg_{0.7}Cu_{0.3}WO_4$ crystals can also be observed from the image.

3.3 Photocatalytic performance

On the basis of the above results, improved photocatalytic activity would be obtained when $Mg_{1-x}Cu_xWO_4$ (x=0.1, 0.2 0.3 and 0.4) and Bi_2WO_6 were combined into heterojunctions. Since $Mg_{0.7}Cu_{0.3}WO_4$ exhibit the highest photocatalytic activity (Fig. S3) among the solid solution samples, the photodegradation of RhB has been investigated to evaluate the photocatalytic activity of as-prepared $Mg_{0.7}Cu_{0.3}WO_4/Bi_2WO_6$ heterojunctions under visible light irradiation. The degradation degree of RhB was examined by determining the change of its characteristic absorption peak at 554 nm. As displayed in Fig. 8a, the pure $Mg_{0.7}Cu_{0.3}WO_4$ and Bi_2WO_6 show relatively poor activity. When $Mg_{0.7}Cu_{0.3}WO_4$ and Bi_2WO_6 were combined to construct $Mg_{0.7}Cu_{0.3}WO_4/Bi_2WO_6$ heterostructures, it can be found that the photocatalytic activities of $Mg_{0.7}Cu_{0.3}WO_4/Bi_2WO_6$ heterojunctions with molar ratio higher than 1:10 is significantly improved compared with pure $Mg_{0.7}Cu_{0.3}WO_4$ and Bi_2WO_6. When the theoretical molar ratio of $Mg_{0.7}Cu_{0.3}WO_4$ to Bi_2WO_6 was 1:4, the highest photocatalytic activity was obtained, resulting in the degradation efficiency of RhB 97.2% after 2 h irradiation. As shown in Fig. 8b, the characteristic absorption peak of RhB at 554 nm decreases with the increase of time, which is consistent with the degradation curve.

Besides, in order to quantitatively understand the reaction kinetics of the photocatalytic degradation process of RhB, a kinetic study was performed by employing the pseudo-first-order model[35,36]:

$$\text{Ln}\ (C_0/C)=k_{app}t \qquad (3)$$

where k_{app} is the apparent pseudo-first-order rate constant (h^{-1}), C_0 is initial RhB concentration (mg/L), C is RhB concentration in aqueous solution at time t (mg/L). Fig. 8c shows RhB photodegradation apparent rate constants of different $Mg_{0.7}Cu_{0.3}WO_4$/ Bi_2WO_6 molar ratio. The experimental data present the corresponding k_{app} values are calculated to be 0.10 h^{-1}, 0.68 h^{-1}, 1.62 h^{-1}, 0.81 h^{-1}, 0.236 h^{-1} and 0.30 h^{-1} for $Mg_{0.7}Cu_{0.3}WO_4/Bi_2WO_6$ with molar ratios 1:0, 1:2, 1:4, 1:6, 1:10 and 0:1, respectively. The results present that 1:4 $Mg_{0.7}Cu_{0.3}WO_4/Bi_2WO_6$ demonstrate the highest k_{app} value (1.62 h^{-1}), which is almost 30 and 5.4 times higher than those of pure $Mg_{0.7}Cu_{0.3}WO_4$ and Bi_2WO_6, respectively, indicating that $Mg_{0.7}Cu_{0.3}WO_4/Bi_2WO_6$ is an excellent composite photocatalyst under visible light.

3.4 Investigation on photocatalytic mechanism

Photoluminescence (PL) emission spectra can serve as an useful approach to investigate the separation and transfer efficiency of photogenerated charge carrier in semiconductor, since PL emission may results from the recombination of free carriers.[37] Generally, the decrease in recombination rate leads to the lower PL intensity, thus higher photocatalytic activity. Fig. 9 presents the PL spectra of the $Mg_{0.7}Cu_{0.3}WO_4/Bi_2WO_6$ composites with molar ratios 1:2, 1:4, 1:6 and1:10 at room temperature. It can be seen that 1:4 $Mg_{0.7}Cu_{0.3}WO_4/Bi_2WO_6$ displays the lowest emission peaks, and thus possess the highest photocatalytic activity which is in good agreement with the result from photodegradation experiment.

Fig. 10a shows the photocurrent of Bi_2WO_6 and 1:4 $Mg_{0.7}Cu_{0.3}WO_4/Bi_2WO_6$ samples generated in electrolyte under visible light, which may indirectly correlate with the generation and transfer of the photoinduced charge carrier in the photocatalytic peocess.[38] As shown in the Figure, the observed photocurrent generation is quite reversible and in good reproducibility, indicating that the electrode is stable. Compared to pure Bi_2WO_6, 1:4 $Mg_{0.7}Cu_{0.3}WO_4/Bi_2WO_6$ exhibits an obviously enhanced photocurrent response, which is about 4 times that of pristine Bi_2WO_6. This remarkablely enhanced photocurrent response further confirmed the more efficient separation and transfer of photoinduced electron−hole pairs occurred in the interface of $Mg_{0.7}Cu_{0.3}WO_4/Bi_2WO_6$ heterojunction.

As the separation and transfer process of charges in the electrode-electrolyte interface region are supposed to be indicated by the electrochemical impedance spectra (EIS) Nyquist plots,[39] the EIS technology can be used to investigate the photocatalytic performance. Fig. 10b shows Nyquist plots of Bi_2WO_6 and 1:4 $Mg_{0.7}Cu_{0.3}WO_4/Bi_2WO_6$ with and without visible light irradiation. It can be seen that the arc radius of 1:4 $Mg_{0.7}Cu_{0.3}WO_4/Bi_2WO_6$ are smaller than Bi_2WO_6, which indicates that the heterojunction possesses a stronger ability in separation and transfer of photogenerated e−h pairs.

To detect the active species during the photodegradation of RhB over $Mg_{0.7}Cu_{0.3}WO_4/Bi_2WO_6$ heterojunctions, trapping experiment was carried out by adding various scavengers to the photodegradation system. We utilized ethylene diamine tetraacetic acid disodium salt (EDTA-2Na), iso-propanol (IPA) and benzoquinone (BQ) as holes (h^+), hydroxyl radicals (•OH) and superoxide radicals (•O_2^-) scavengers, respectively.[25,26] It can be seen that the photodecomposition of RhB was almost not affected by adding IPA. In contrast, the degradation efficiency of RhB was inhibited about 100% and 80% with the addition of EDTA-2Na and BQ, respectively (Fig. 11a). Thus, it can be supposed that photogenerated holes (h^+) and •O_2^- are the main active species of $Mg_{0.7}Cu_{0.3}WO_4/Bi_2WO_6$ for RhB degradation under visible light irradiation.

To further understand the change of active species over $Mg_{0.7}Cu_{0.3}WO_4/Bi_2WO_6$ heterojunction, the detailed •O_2^- quantification experiments have been carried out. Fig. 11b shows the absorption spectra centered at 259 nm of NBT under visible light irradiation (λ > 420 nm) for 4 h during the photocatalytic reaction. It is obvious that the absorption peak gradually decreased as increasing the irradiation time, which confirms that the •O_2^- play important role in the photocatalytic reaction over $Mg_{0.7}Cu_{0.3}WO_4/Bi_2WO_6$ heterojunctions. It further demonstrates that in $Mg_{0.7}Cu_{0.3}WO_4/Bi_2WO_6$ heterojunction (Scheme 1), the photogenerated electrons on $Mg_{0.7}Cu_{0.3}WO_4$ could easily transfer to Bi_2WO_6, leading more photogenerated electrons react with O_2

to produce •O_2^- and take part in decomposition of RhB. Meanwhile, the holes (h^+) migrate from Bi_2WO_6 to the VB of $Mg_{0.7}Cu_{0.3}WO_4$, making charge separation more efficient and reducing the recombination probability, which is in good agreement with the photocatalytic activity.

4. Conclusions

In summary, energy-levels well-matched $Mg_{0.7}Cu_{0.3}WO_4/Bi_2WO_6$ heterojunctions have been successfully constructed through semiconductor band gap engineering based on solid-solution design and synthesized by a facile hydrothermal method. The as-designed $Mg_{0.7}Cu_{0.3}WO_4/Bi_2WO_6$ heterojunctions consisting of nanocubes and nanoplates structures exhibit highly improved visible-light-driven photocatalytic performance compared to pure samples. It was also confirmed by the photoelectrochemical measurements. The optimum photocatalytic activity of the 1:4 $Mg_{0.7}Cu_{0.3}WO_4/Bi_2WO_6$ sample for the degradation of RhB was almost 30 and 5.4 times higher than those of pristine $Mg_{0.7}Cu_{0.3}WO_4$ and Bi_2WO_6, respectively. Active species trapping and quantification measurements indicated that superoxide radicals (•O_2^-) and photogenerated holes (h^+) play a crucial role in photodegradation of RhB over $Mg_{0.7}Cu_{0.3}WO_4/Bi_2WO_6$ heterojunctions. The fabrication of well-matched overlapping band-structures can result in efficient photogenerated-charges transfer between $Mg_{0.7}Cu_{0.3}WO_4$ and Bi_2WO_6, enhancing the VLD photocatalytic reactivity.

Acknowledgement

This work was supported by the Fundamental Research Funds for the Central Universities (2652013052), and the National Natural Science Foundation of China under Grants 50590402, and 91022036, and the National Basic Research Project of China (2010CB630701, and 2011CB922204).

Notes and references

[a] *National Laboratory of Mineral Materials, School of Materials Science and Technology, China University of Geosciences, Beijing, 100083, PR China, Tel: 86-10-82332247; E-mail: hhw@cugb.edu.cn; zyh@cugb.edu.cn.*

[b] *Department of Physics and Materials Science, City University of Hong Kong, Tat Chee Avenue, Kowloon, Hong Kong, China*

† Electronic Supplementary Information (ESI) available: [Diffuse reflectance spectra of Bi_2WO_6, CB and VB of $Mg_{1-x}Cu_xWO_4$, SEM image of and ICP elemental analysis of $Mg_{0.7}Cu_{0.3}WO_4/Bi_2WO_6$ heterojunction and photocatalytic degradation curves of $Mg_{1-x}Cu_xWO_4$ samples]. See DOI: 10.1039/b000000x/

1 M. W. Kanan and D. G. Nocera, *Science.* 2008, **321,** 1072.
2 A. Kubacka, M. Fernández-García and G. Colón, *Chem. Rev.* 2012, **112,** 1555.
3 H. Tong, S. X. Ouyang, Y. P. Bi, N. Umezawa, M. Oshikiri and J. H. Ye, *Adv. Mater.* 2012, **24,** 229.
4 A. L. Linsebigler, G. Lu and J. T. Yates, *Chem. Rev.* 1995, **95,** 735.
5 X. Chen and S. S. Mao, *Chem. Rev.* 2007, **107,** 2891.
6 F. Z. Liu, Y. H. Leung, A. B. Djurišić, A. M. Ching Ng and W. K. Chan, *J. Phys. Chem. C*, 2013, **117,** 12218.
7 Q. Li, H. Meng, P. Zhou, Y. Q. Zheng, J. Wang, J. G. Yu and J. R. Gong, *ACS Catal.* 2013, **3,** 882.
8 H. W. Huang, Y. He, Z. S. Lin, L. Kang and Y. H. Zhang, *J. Phys. Chem. C*, 2013, **117,** 22986.
9 J. Cao, B. Xu, B. Luo, H. Lin, S. Chen, *Catal. Commun.* 2011, **13,** 63.
10 L. Q. Ye, J. Y. Liu, Z. Jiang, T. Y. Peng and L. Zan, *Appl. Catal., B* 2013, **142,** 1.
11 T. H. Yu, W. Y. Cheng, K. J. Chao, S. Y. Lu, *Nanoscale.* 2013, **5,** 7356.
12 H. Cheng, B. Huang, Y. Dai, X. Qin, X. Zhang, Z. Wang and M. Jiang, *J. Solid State Chem.* 2009, **182,** 2274.
13 M. Ge, Y. Li, L. Liu, Z. Zhou and W. Chen, *J. Phys. Chem. C* 2011, **115,** 5220.
14 R. Shi, G. L. Huang, J. Lin and Y. F. Zhu, *J. Phys. Chem. C* 2009, **113,** 19633.
15 Y. Fu, C. Chang, P. Chen, X. L. Chu and L. Y. Zhu, *J. Hazard. Mater.* 2013, **254,**185.
16 S. Guo, X. F. Li, H. Q. Wang, F. Dong and Z. B. Wu, *J. Colloid Interf. Sci.* 2012, **369,** 373.
17 Y. Tian, L. D. Zhang and J. X. Zhang, *J. Alloys Compd.* 2012, **537,** 24.
18 M. Shang, W. Z. Wang, L. Zhang, S. M. Sun, L. Wang and L. Zhou, *J. Phys. Chem. C* 2009, **113,** 14727.
19 D. Q. He, L. L. Wang, D. D. Xu, J. L. Zhai, D. J. Wang and T. F. Xie, *ACS Appl. Mater. Interfaces* 2011, **3,** 3167.
20 M. S. Gui, W. D. Zhang, Y. Q. Chang and Y. X. Yu, *Chem. Eng. J.* 2012, **197,** 283.
21 H. Q. Li, Y. M. Cui and W. S. Hong, *Appl. Surf. Sci.* 2013, **264,** 581.
22 Y. L. Tian, B. B. Chang, J. L. Lu, J. Fu, F. N. Xi and X. P. Dong, *ACS Appl. Mater. Interfaces.* 2013, **5,** 7079.
23 H. W. Huang, S. B. Wang, Na. Tian, Y. H. Zhang, *RSC Advance*, 2014, **4,** 5561.
24 J. E. Yourey, K. J. Pyper, J. B. Kurtz and B. M. Bartlett, *J. Phys. Chem. C* 2013, **117,** 8708.
25 L. Ye, J. Liu, C. Gong, L. Tian, T. Peng and L. Zan, *ACS Catal.* 2012, **2,** 1677.
26 X. J. Bai, L. Wang and Y. F. Zhu, *ACS Catal.* 2012, **2,** 2769.
27 X. Zhang, Z. H. Ai, F. L. Jia and L. Z. Zhang, *J. Phys. Chem. C* 2008, **112,** 747.
28 J. E. Yourey, J. B. Kurtz and B. M. Bartlett, *Inorg. Chem.* 2012, **51,** 10394.
29 L. W. Zhang, Y. Man and Y. F. Zhu, *ACS Catal.* 2011, **1,** 841.
30 Y. Ohko, K. Hashimoto and A. Fujishima, *J. Phys. Chem. A.* 1997, **101,** 8057.
31 Y. G. Su, B. L. Zhu, K. Guan, S. S. Gao, L. Lv, C. F. Du, L. M. Peng, L. C. Hou and X. J. Wang, *J. Phys. Chem. C* 2012, **116,** 18508.
32 H. Liu, W. R. Cao, Y. Su, Y. Wang and X. H. Wang, *Appl. Catal. B* 2012, **111,** 271.
33 J. S. Corneille, J. W. He and D. W. Goodman, *Surf. Sci.* 1994, **306,** 269.
34 J. Morales, L. Sánchez, F. Martín, J. R. Ramos-Barrado, M. Sánchez, *Thin Solid Films.* 2005, **474,** 133.
35 C. H. Wu, H. W. Chang and J. M. Chern, *J. Hazard. Mater.* 2006, **137,** 336.
36 Y. He, Y. H. Zhang, H. W. Huang, N. Tian and Y. Luo, *Inorg. Chem. Comm.* 2014, **40,** 55.
37 X. J. Wang, Q. Wang, F. T. Li, W. Y. Yang, Y. Zhao, Y. J. Hao and S. J. Liu, *Chem. Eng. J.* 2013, **234,** 361.
38 H. Kim, P. Borse, W. Choi and J. Lee, *Angew. Chem., Int. Ed.* 2005, **44,** 4585.
39 Z. Hosseini, N. Taghavinia, N. Sharifi, M. Chavoshi and M. Rahman, *J. Phys. Chem. C* 2008, **112,** 18686.

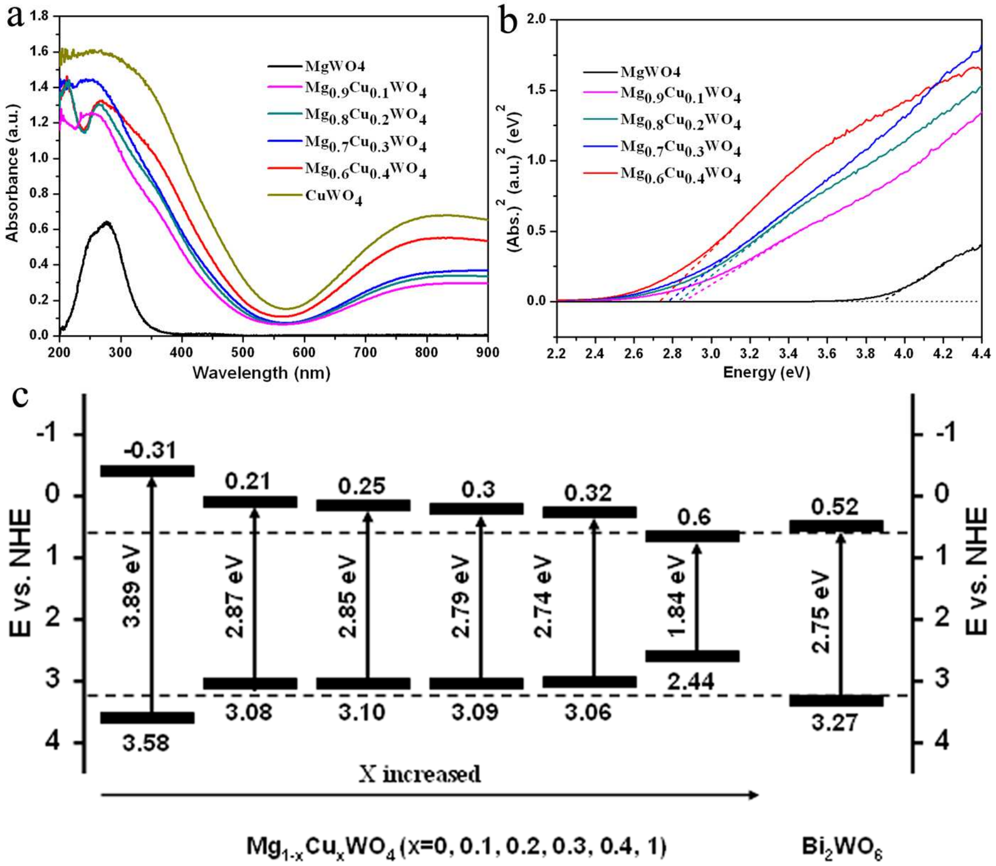

Fig. 1 (a) UV-vis diffuse reflectance spectra and (b) the band gap energies of $Mg_{1-x}Cu_xWO_4$ (x=0, 0.1, 0.2 0.3 0.4 and 1) samples. (c) The comparison of energy levels of $Mg_{0.7}Cu_{0.3}WO_4$ (x=0, 0.1, 0.2 0.3 0.4 and 1) and Bi_2WO_6.

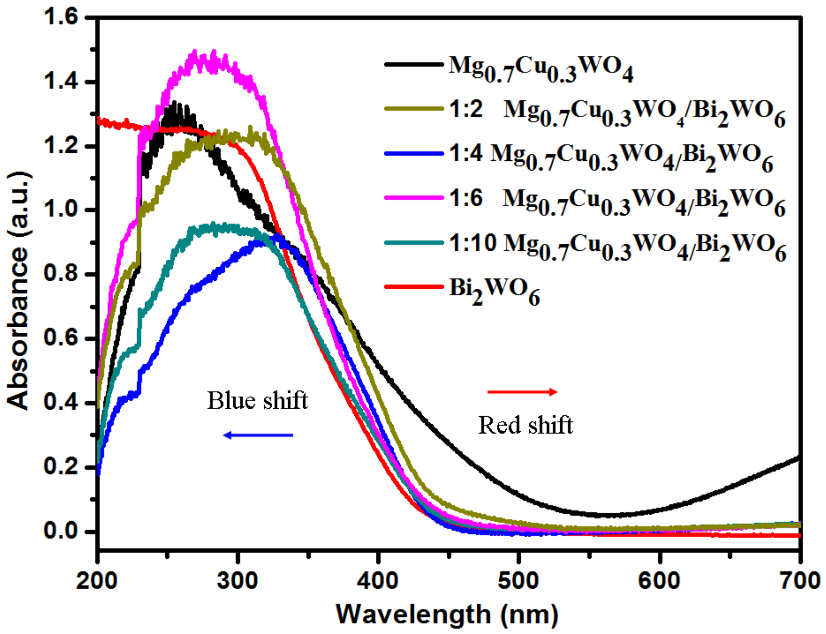

Fig. 2 UV-vis diffuse reflectance spectra of $Mg_{0.7}Cu_{0.3}WO_4/Bi_2WO_6$ with different molar ratios.

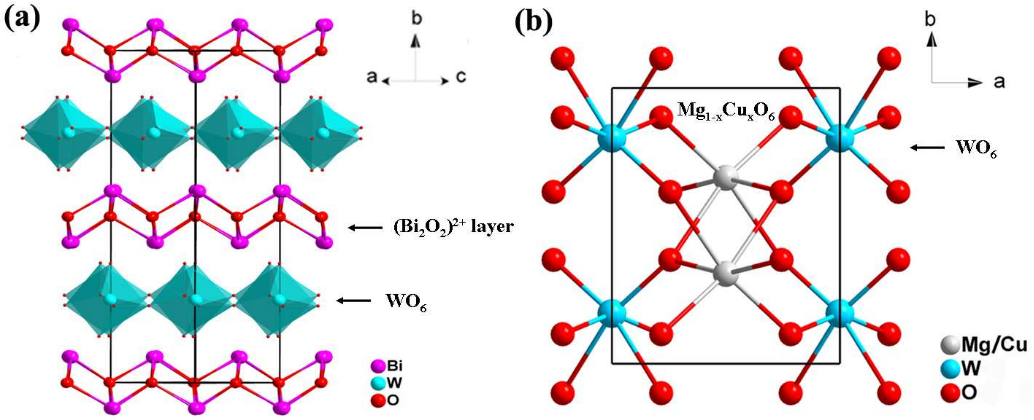

Fig. 3 Crystal structure of (a) orthorhombic phase Bi_2WO_6 and (b) monoclinic phase $Mg_{0.7}Cu_{0.3}WO_4$.

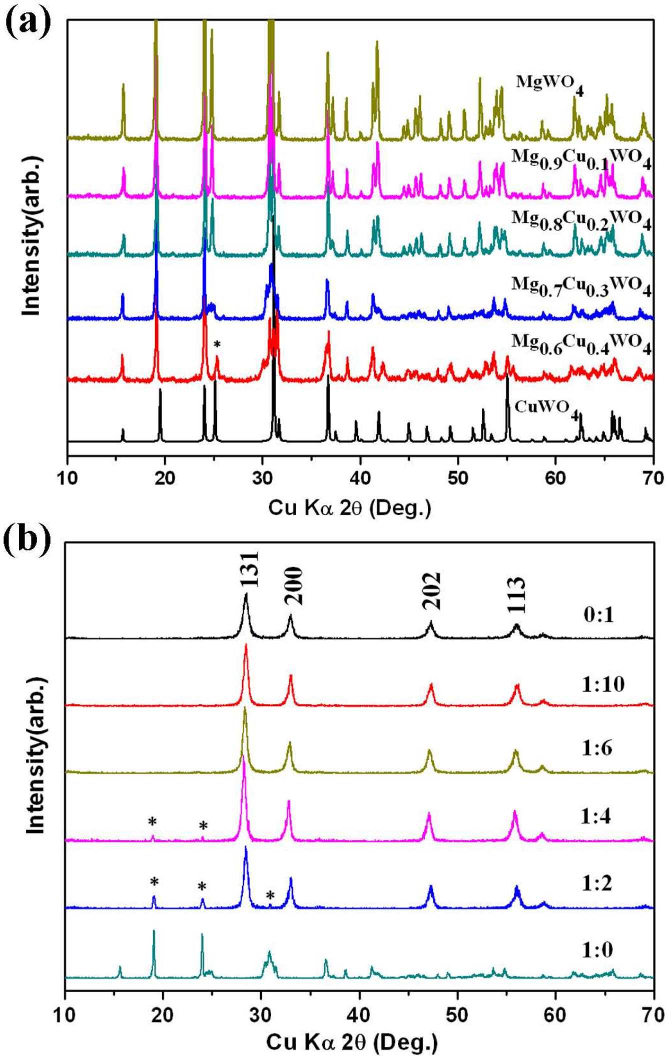

Fig. 4 XRD patterns of (a) $Mg_{1-x}Cu_xWO_4$ (x=0, 0.1, 0.2, 0.3, 0.4 and 1) and (b) $Mg_{0.7}Cu_{0.3}WO_4/Bi_2WO_6$ with molar ratios 0:1, 1:10, 1:6, 1:4, 1:2 and 1:0.

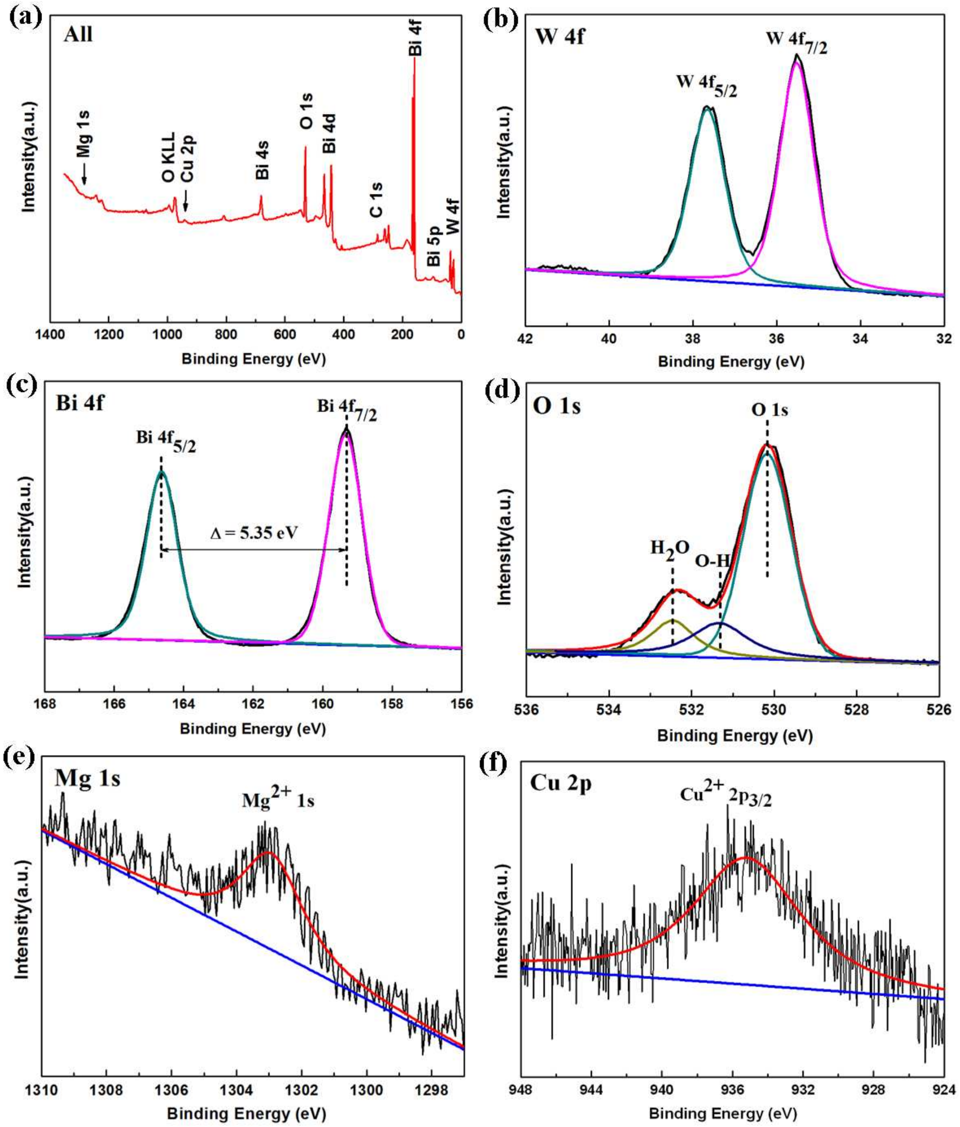

Fig. 5 XPS spectra of the 1:4 $Mg_{0.7}Cu_{0.3}WO_4/Bi_2WO_6$ heterostructures: (a) survey, (b) W 4f, (c)Bi 4f, (d) O 1s, (e) Mg 1s and (f) Cu 2p.

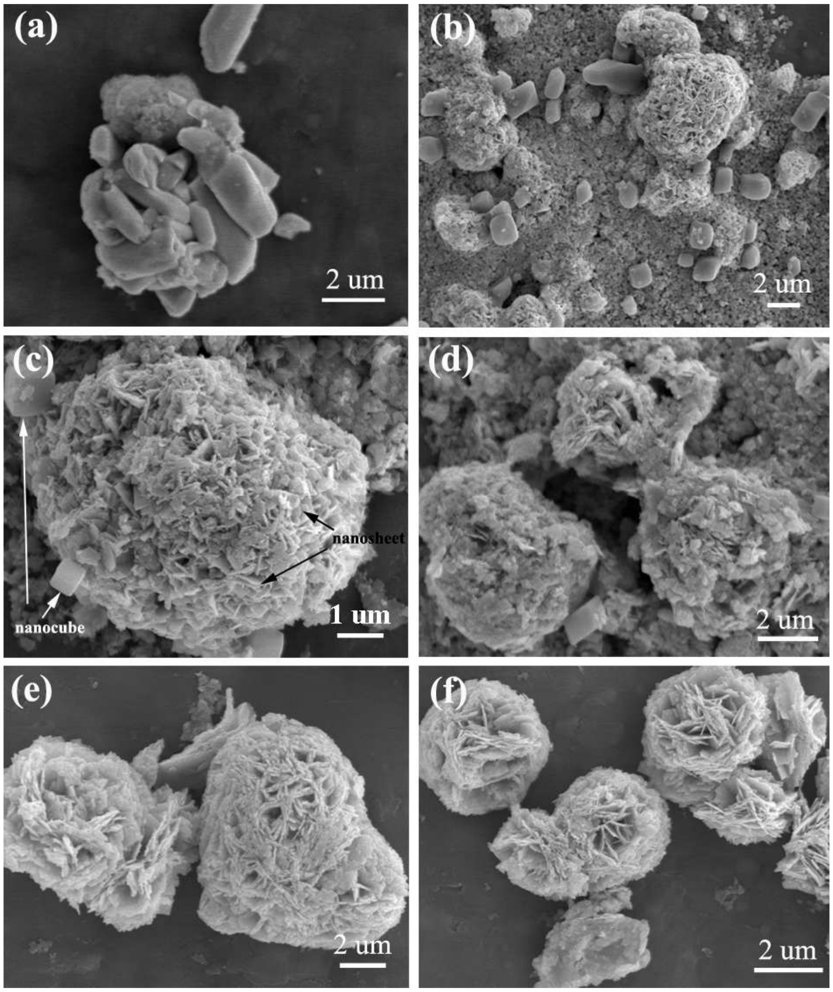

Fig. 6 SEM images of as-prepared products with $Mg_{0.7}Cu_{0.3}WO_4/Bi_2WO_6$ molar ratios: (a) 1:0, (b) 1:2, (c) 1:4, (d) 1:6, (e) 1:10 (f) 0:1.

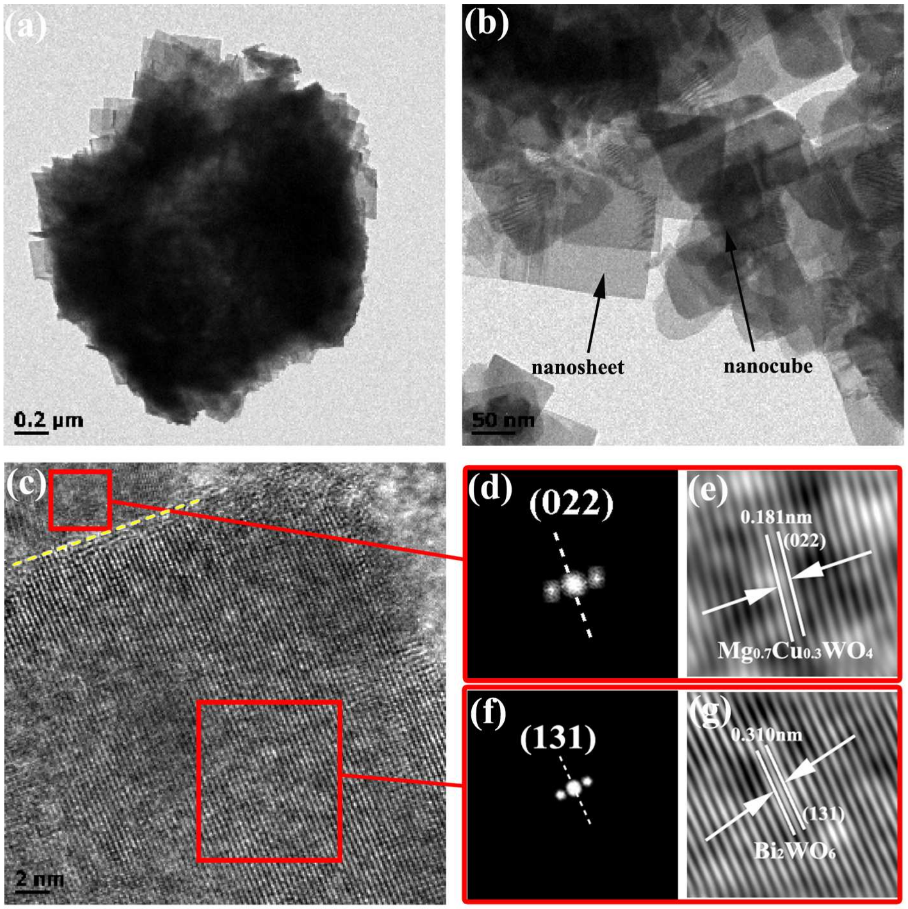

Fig. 7 (a,b) TEM, (c) HRTEM images, (d, f) FFT (fast Fourier transition) patterns and (e, g) inverse FFT (fast Fourier transition) patterns of the lattice fringe of $Mg_{0.7}Cu_{0.3}WO_4/Bi_2WO_6$ heterostructures.

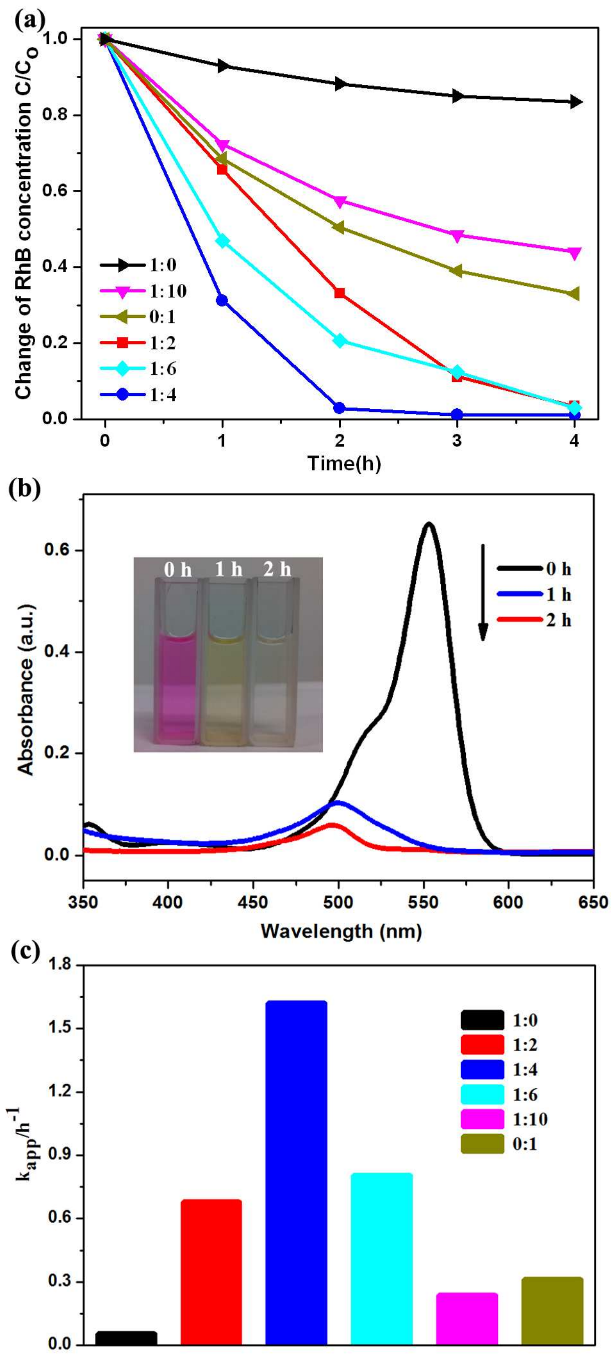

Fig. 8 (a) Photocatalytic degradation curves of RhB under the irradiation of visible light. (b) Temporal absorption spectral patterns of RhB during the photodegradation process of 1:4 $Mg_{0.7}Cu_{0.3}WO_4/Bi_2WO_6$. (c) Apparent rate constants for the photodegradation of RhB over $Mg_{0.7}Cu_{0.3}WO_4/Bi_2WO_6$ with different molar ratios.

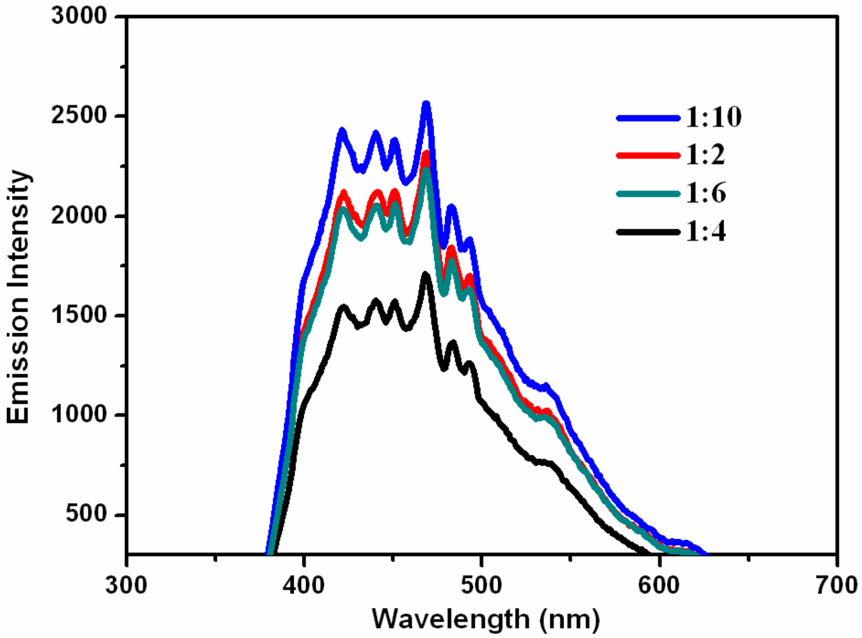

Fig. 9 PL spectra of $Mg_{0.7}Cu_{0.3}WO_4/Bi_2WO_6$ with molar ratios 1:2, 1:4, 1:6 and 1:10.

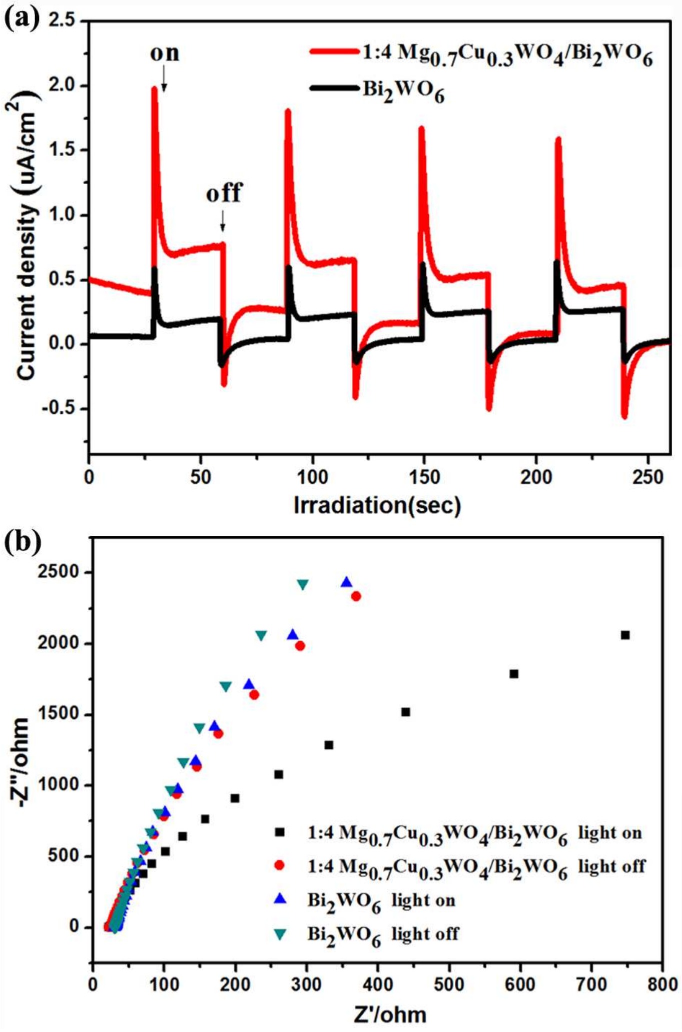

Fig. 10 (a) Comparison of transient photocurrent response and (b) EIS Nynquist plots of the Bi_2WO_6 and 1:4 $Mg_{0.7}Cu_{0.3}WO_4/Bi_2WO_6$ with light on/off cycles under the irradiation of visible-light irradiation ($\lambda > 420$ nm, [Na_2SO_4] = 0.1 M).

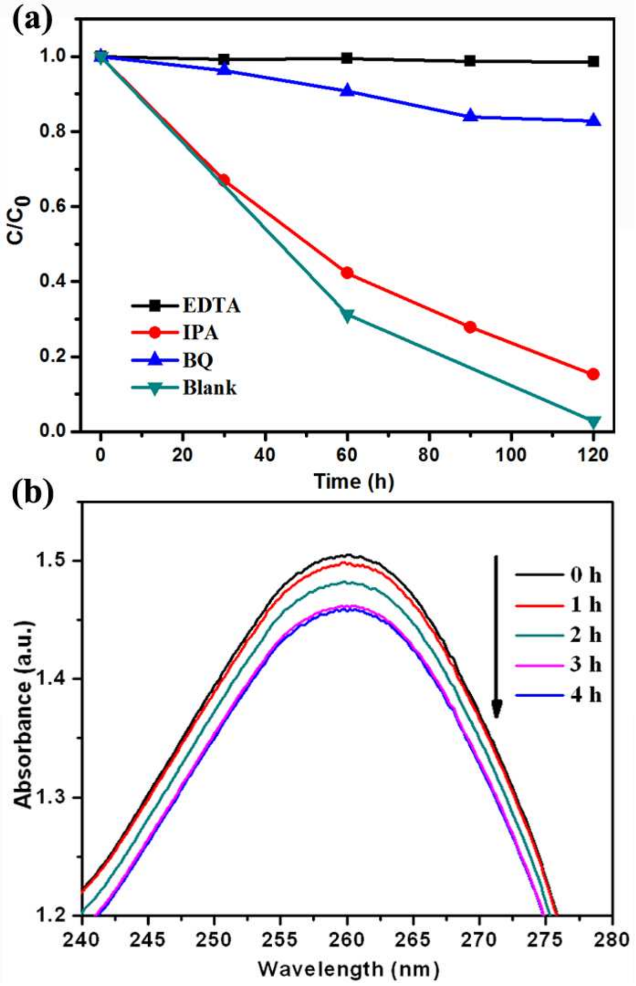

Fig. 11 (a) Photodegradation of RhB over 1:4 $Mg_{0.7}Cu_{0.3}WO_4/Bi_2WO_6$ in the presence of different scavengers. (b) Absorption spectra of NBT with 4 h visible light irradiation (λ > 420 nm).

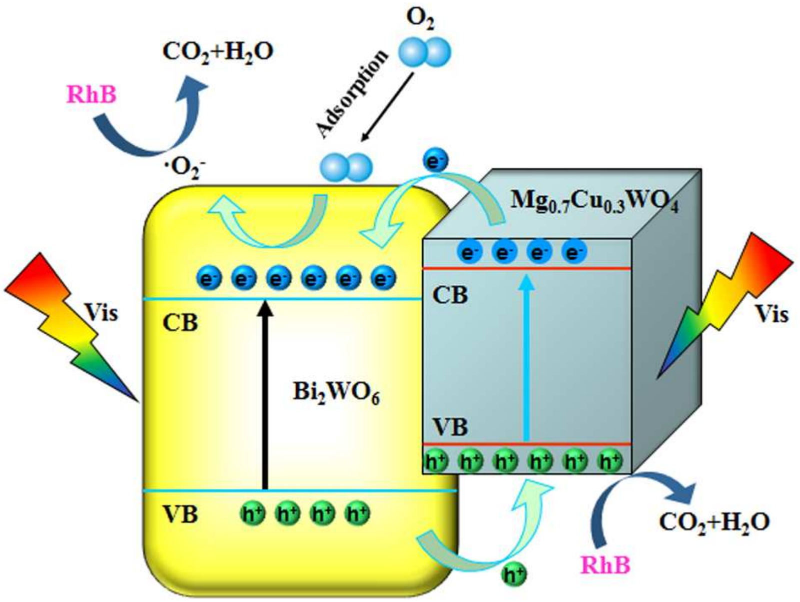

Scheme 1 Schematic diagrams of $Mg_{0.7}Cu_{0.3}WO_4/Bi_2WO_6$ heterostructures under visible light irradiation.

Band Gap Engineering Design for Construction of Energy-levels Well-matched Semiconductor Heterojunction with Enhanced Visible-light-driven Photocatalytic Activity

Hongwei Huang*,†, Shuobo Wang†, Yihe Zhang*,†, Paul K. Chu‡

† National Laboratory of Mineral Materials, School of Materials Science and Technology, China University of Geosciences, Beijing, 100083, PR China

‡ Department of Physics and Materials Science, City University of Hong Kong, Tat Chee Avenue, Kowloon, Hong Kong, China

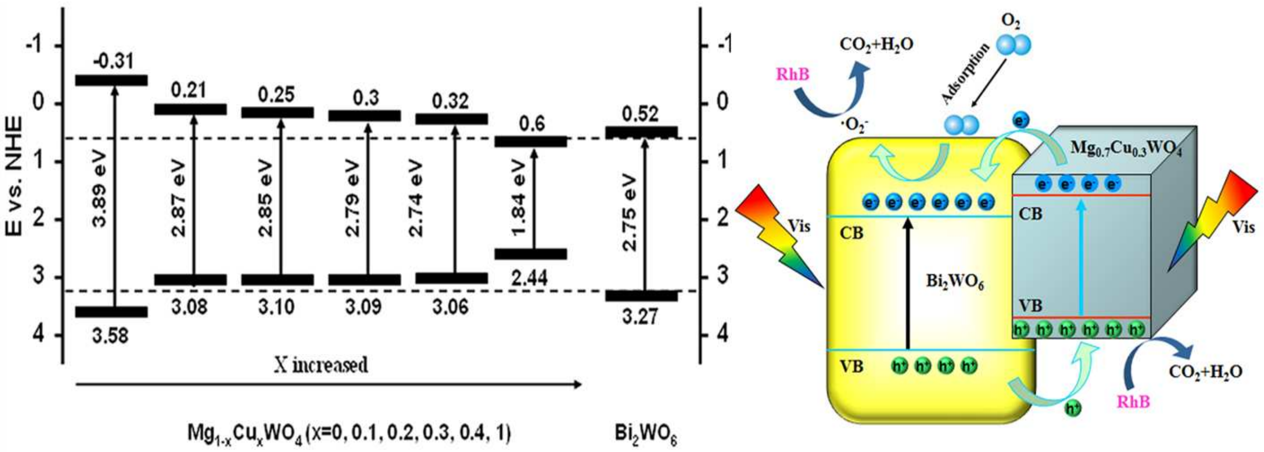

Energy-levels well-matched $Mg_{1-x}Cu_xWO_4/Bi_2WO_6$ heterojunctions were successfully constructed based on band gap engineering design. It exhibits high visible-light-driven photocatalytic activity for degradation of RhB and photocurrent generation.